2024 23rd IEEE Intersociety Conference on Thermal and Thermomechanical Phenomena in Electronic Systems (ITherm) | 979-8-3503-6433-0/24/$31.00 ©2024 IEEE | DOI: 10.1109/ITherm55375.2024.10709503

Performance Assessment of Hybrid Microchannel-Pin Fin Heat Sink for Hotspot Thermal Management Under Flow Boiling Conditions

Amitav Tikadar, Satish Kumar
G.W. Woodruff School of Mechanical Engineering, Georgia Institute of Technology, Altanta, GA 30332, USA
satish.kumar@me.gatech.edu

***Abstract*—Two-phase microchannel heat sinks are widely used for miniature microelectronic cooling due to their significantly high heat transfer coefficients. However, in complex heterogeneous 2.5D and 3D integrated circuit (IC) architectures, conventional plate-fin microchannel heat sinks often fail to provide uniform cooling across the localized high heat-flux hotspots and low heat-flux background zones owing to their limited heat transfer surface area and eventually result in high temperature gradient, high thermal stress, and ultimate failure. To address this challenge, this paper introduces a novel hybrid microchannel-pin fin heat sink layout consisting of parallel plate-fin microchannels over the background zone and clustered pin fins over the hotspot zone. The clustered pin fins locally increase the surface area in the hotspot region, while parallel plate fins over the background zone ensure uniform coolant flow and avoid flow bypassing around the clustered pin fins. Moreover, parallel plate fins upstream of the hotspot effectively suppress flow boiling instability. A coupled three-dimensional (3D) volume-of-fluid (VOF) and phased-change model has been developed to assess the thermal-hydraulic performance of the proposed hybrid microchannel-pin fin heat sink under flow boiling conditions over a wide range of hotspot heat flux using saturated water as coolant. The flow boiling performance of the hybrid microchannel-pin fin heat sink has also been compared with the conventional plate-fin microchannel heat sink. The results obtained from the developed numerical model reveal that the proposed hybrid microchannel-pin fin heat sink layout effectively dissipates both background and hotspot heat fluxes and subsequently, enhances temperature uniformity across the hotspot and background zones with a marginal increment in pressure drop compared to the conventional microchannel heat sink. The numerical model provides deep insights into the bubble dynamics and corresponding transient thermal-hydraulic response, which can be used for the optimization of the hybrid microchannel-pin fin heat sink layout.**

Keywords—microchannel, pin fins, plate fins, flow boiling, heat sink, microelectronics, hotspot.

I. INTRODUCTION

In the rapidly advancing landscape of electronic devices, efficient thermal management is extremely important to ensure optimal performance, reliability, and longevity. Conventional single-phase mini and micro-channel heat sinks or pin fin heat sink are often used for miniature micro-electronic cooling because of their high surface area to volume ratio, high heat transfer coefficient, reliability, and predictability [1]. However, these single-phase microfluidic cooling solutions are inadequate for ultra-high-heat-flux generating next-generation microprocessors and power electronics due to their high temperature gradient along the stream-wise direction of the coolant and the consequent high thermal stress [2].

Latent heat driven two-phase heat sinks, i.e., flow boiling heat sinks, provide significantly high heat transfer coefficient with minimal coolant flow rate and provide better stream-wise temperature uniformity than single-phase heat sinks and hence, can be used for next-generation microelectronics cooling [3]. To date, many researchers have not only extensively studied different fundamental aspects of flow boiling heat transfer in micro and mini-channels and pin fin heat sinks, such as flow boiling patterns [4] and boiling instability [5-6], but also studied different flow boiling enhancement techniques such as inlet restriction [7], surface roughness [8], and auxiliary jetting [9]. For example, Mudawar et al. [10] experimentally characterized the fundamental saturated flow boiling phenomenon in a water-cooled microchannel heat sink under different mass flux, heat flux, and sub-cooling conditions. Kandlikar et al. [11] achieved a critical heat flux (CHF) of 1070 $W.cm^{-2}$ using a tapered gap micro-channel heat sink.

Although conventional two-phase heat sinks may provide sufficient cooling for uniformly heated devices, however, for highly non-uniform heat flux generating heterogeneous 2.5D and vertically stacked 3D ICs, conventional heat sink fails to provide sufficiently uniform cooling. Therefore, to tackle highly non-uniform heat flux distributions while ensuring temperature uniformity, hotspot-specific multi-zone cooling solution is needed. To this end, Joshi et al. [12-13] designed a silicon (Si) microgap enhanced with pin fins over the low heat flux background zone and densely packed clustered pin fins over to the hotspot zone to locally increase the surface area and subsequently achieved notably high temperature uniformity across the background and hotspot zones under a wide range of heterogeneous heating conditions. However, significantly high pressure drop and flow bypass around the densely packed fin cluster may outweigh the thermal benefits of the variable pin fin cluster design. For hotspot thermal management, Ansari et al. [14] proposed an interesting concept of a hybrid microchannel-pin fin heat sink design where microchannels are placed over the background zone, and cylindrical pin fins are placed over the hotspot zone. The authors numerically demonstrated that the single-phase hybrid microchannel-pin fin heat sink provides enhanced temperature uniformity under

Authorized licensed use limited to: Institut Teknologi Sepuluh Nopember. Downloaded on November 02,2026 at 03:10:37 UTC from IEEE Xplore. Restrictions apply.

heterogeneous heat flux conditions. However, the thermal-hydraulic performance of the hybrid heat sink under flow boiling conditions has yet to be investigated. Similarly, Kumar et al. [15] proposed a hybrid microchannel-metal foam heat sink where rectangular microchannels and metal foams are deployed over the background and hotspot zones, respectively. Although the authors reported enhanced thermal performance using single-phase coolant, the thermal-hydraulic performance of the hybrid microchannel-metal foam heat sink under flow boiling conditions remains unexplored.

From the above literature survey, it is evident that a specialized hotspot-specific multi-zone cooling solution is imperative for heterogeneous ICs. Therefore, in this paper, a two-phase hybrid microchannel-pin fin heat sink consisting of parallel plate-fin microchannels over the background zone and clustered pin fins over the hotspot zone has been designed, inspired from the single-phase hybrid heat sink design proposed by Ansari et al. [14], to enhance temperature uniformity under heterogeneous heating profile with minimal pumping cost. The flow boiling performance of the designed hybrid microchannel-pin fin heat sink layout has been numerically investigated with a wide range of heterogeneous heat flux conditions. Moreover, the flow boiling performance of the hybrid heat sink has also been compared with the conventional plate-fin microchannel heat sink, considering the spatio-temporal bubble dynamics and the corresponding transient thermal-hydraulic response.

II. Heat Sink Designs

A. Conventional Microchannel Heat Sink

In this paper, a silicon (Si) microchannel heat sink has been considered with an overall background footprint of 10.5×10 mm^2, as shown in Fig. 1. The heat sink is composed of 25 microchannels, each having a cross-sectional area of 250×250 µm^2 and the channels are separated by 150 µm thick walls. The bottom surface of the heat sink is divided into three zones to facilitate heterogeneous heating: a 10×0.5mm^2 adiabatic entrance zone, a 10×10 mm^2 background zone (based on typical die size), and a 0.5×0.5 mm^2 hotspot zone located in the middle of the background zone (see Fig. 1(b)). The

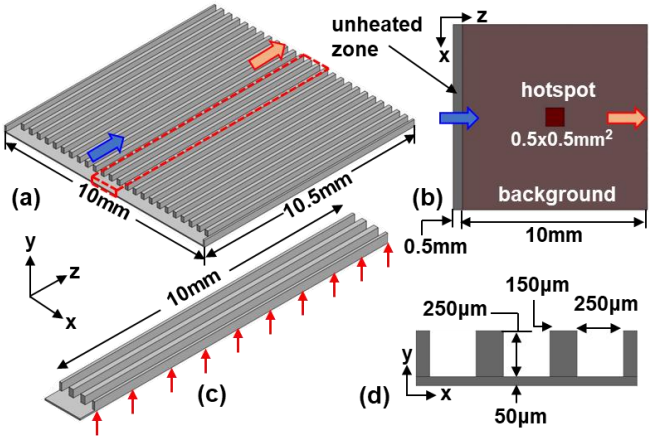

Figure 1: (a) Schematic of a conventional microchannel heat sink, (b) bottom view of the heat sink with different heating zones, (c) considered computational domain for numerical modeling, and (d) front view of the computational domain with relevant dimensions.

background zone is heated with a constant heat flux (q''_{bg}) of 30 W.cm^{-2}, whereas the hotspot zone is heated with a range of high heat flux (q''_{hs}) from 60 to 120 W.cm^{-2}. Detailed specifications of the microchannel heat sink have been shown in the Fig. 1. It is worth mentioning that saturated water has been considered as the coolant, flowing along +z direction to extract heat from the heat sink.

B. Hybrid Microchannel-Pin Fin Heat Sink

In order to enhance the temperature uniformity by efficiently extracting heat from the high heat-flux generating hotspot zone with minimal pumping cost, the conventional microchannel heat sink has been modified with an array of cylindrical micro pin-fins only over the hotspot zone to locally increase the surface area, as shown in Fig. 2. It is worth mentioning that pin fins have been arranged in staggered fashion with identical longitudinal and transverse pitches of 112 µm to enhance the flow boiling performance. Moreover, the height of the pin fins was the same as the microchannel height of 250 µm. Detailed specifications of the staggered pin fins have been shown in the Fig. 2(c).

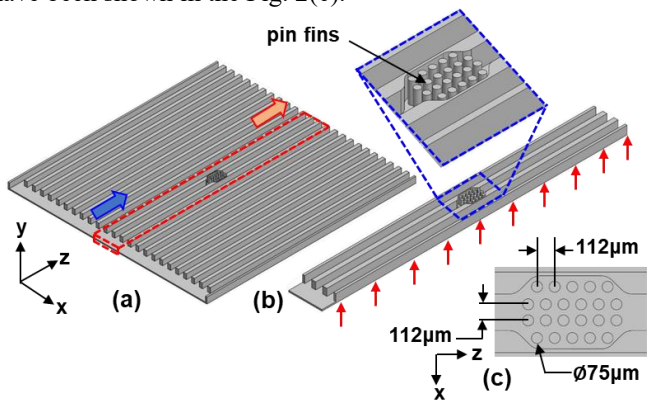

Figure 2: (a) Schematic of a microchannel-pin fin heat sink, (b) computational domain for numerical modeling, and (c) top view of the pin fins with relevant dimensions.

III. Mathematical Model for Flow Boiling

In order to reduce the computational cost while capturing the effect of full hotspot and the clustered pin fins on the flow boiling performance of the heat sink, only three micro-channels, the corresponding plate/pin fins, and substrate have been considered as computational domain for the computational fluid dynamics and heat transfer (CFD/HT) analysis for both the conventional microchannel and hybrid microchannel-pin fin heat sinks, as shown in the Fig. 1(c-d) and 2(b), respectively. Moreover, the following assumptions have been made to further simplify the CFD/HT model: (1) transient incompressible laminar flow, (2) negligible radiation heat transfer and viscous dissipation, (3) constant thermo-physical properties except the thermal conductivity (k) of the Si, and (4) water saturation temperature is constant at 100°C.

Considering the aforementioned assumptions, in this study, a coupled volume of fluid (VOF) and a mechanistic phase change model have been developed to assess the thermal-hydraulic performance of the proposed heat sinks under flow boiling conditions.

Authorized licensed use limited to: Institut Teknologi Sepuluh Nopember. Downloaded on November 02,2026 at 03:10:37 UTC from IEEE Xplore. Restrictions apply.

A. Volume of Fluid (VOF) Model

The VOF model is an interface tracking technique designed to capture interfaces between multiple immiscible fluids. In this model, all fluids are governed by a single momentum equation that resolve the volume fraction of each phases within an individual grid-cell in the computational domain. The dynamic tracking of interfaces is achieved by solving the continuity equation for volume fractions of liquid and vapor phases.

For two-phase flow, the mass continuity equations for the liquid and vapor phases are expressed as follows:

$$\frac{\partial}{\partial t}(\alpha_l \rho_l) + \nabla.(\alpha_l \rho_l \vec{v}) = S_l \quad (1)$$

$$\frac{\partial}{\partial t}(\alpha_v \rho_v) + \nabla.(\alpha_v \rho_v \vec{v}) = S_v \quad (2)$$

Where, α is volume fraction, ρ is density, $\vec{v}$ is velocity vector, and S is the source term that represents the mass transfer rate between two phases per unit volume due to evaporation and condensation. The subscripts l and v represent the liquid and vapor phases, respectively.

Moreover, the sum of liquid and vapor phase mass fractions must equal to unity:

$$\alpha_l + \alpha_v = 1 \quad (3)$$

In the VOF model, a single momentum conservation is solved as shown in the following equation, which is shared by both the liquid and vapor phases:

$$\frac{\partial}{\partial t}(\rho \vec{v}) + \nabla.(\rho \vec{v} \vec{v}) = -\nabla P + \nabla[\mu \nabla \vec{v} + \nabla \vec{v}^T] + \rho \vec{g} + \vec{F} \quad (4)$$

Where, P is the pressure, μ is the dynamic viscosity, g is the gravity, and $\vec{F}$ is the body force. The mixture ρ and μ terms are weighted by each phase α as follows:

$$\rho = \alpha_l \rho_l + \alpha_v \rho_v \quad (5)$$

$$\mu = \alpha_l \mu_l + \alpha_v \mu_v \quad (6)$$

Moreover, the continuum surface force (CSF) model has been used to calculate the surface tension force between the liquid and vapor phases. According to the Young-Laplace equation, the pressure drop across the curved surface between two fluids depends on the surface tension coefficient (σ) and the surface curvature as measured by two radii in orthogonal directions:

$$\nabla P = \sigma \left(\frac{1}{R_1} + \frac{1}{R_2}\right) \quad (7)$$

Afterward, body force $(\vec{F})$ terms of the momentum equation can be calculated as follows by manipulating Eq. (7) using the divergence theorem:

$$\vec{F} = \sigma \frac{\rho \kappa \nabla \alpha_v}{0.5(\rho_l + \rho_v)} \quad (8)$$

Where, κ is the interface curvature.

The contact angle between the solid wall and generated vapor phase is used to compute the curvature of the vapor phase near the solid domain, which allows the inclusion of surface wettability effects. The surface normal in adjacent cells to the wall is calculated as follows:

$$\hat{n} = \hat{n}_w \cos\theta_w + \hat{t}_w \sin\theta_w \quad (9)$$

Where, $\hat{n}_w$ and $\hat{t}_w$ are the unit vectors normal and tangential to the wall, respectively and θ_w is the contact angle at the wall. In this study, a θ_w of 90° has been used, as experimentally measured by Arkles et al. [16] for etched Si and water.

In VOF, a shared energy equation for both phases is solved as follows:

$$\frac{\partial}{\partial t}(\rho E) + \nabla[\vec{v}(\rho E + P)] = \nabla(k \nabla T) + S_e \quad (10)$$

Where, E and T are the mass-average mixture energy and temperature, k is the phase-average thermal conductivity, S_e is the volumetric source term representing the energy exchange between the liquid and vapor phases via evaporation and condensation.

Moreover, the mass average E of both the liquid and vapor phases has been calculated as follows:

$$E = \frac{\alpha_l \rho_l E_l + \alpha_v \rho_v E_v}{\alpha_l \rho_l + \alpha_v \rho_v} \quad (11)$$

B. Phase Change Model

In this paper, the widely accepted mechanistic phase change model proposed by Lee has been used to calculate the mass transfer, i.e., S_l and S_v during flow boiling process as a function of the local and saturation temperature difference:

$$S_l = -\lambda_l \alpha_l \rho_l \frac{T_l - T_{sat}}{T_{sat}}, T_l \geq T_{sat} \quad (12)$$

$$S_v = -\lambda_l \alpha_v \rho_v \frac{T_v - T_{sat}}{T_{sat}}, T_v < T_{sat} \quad (13)$$

Where, λ_l and λ_v are the relaxation factors that need to be tuned appropriately, and T_{sat} is the saturation temperature of the water, which is assumed to be constant at 100°C. In this study, both λ_l and λ_v are set to 0.5 s^{-1}, as suggested by Yong et al [17], to reduce the temperature fluctuations at the interface and also to ensure numerical stability.

The corresponding heat transfer associated with the mass transfer process has been calculated as follows:

$$S_e = S_i h_{lv} \quad (14)$$

Where, S_i is the mass source term, and h_{lv} is the latent heat of vaporization.

C. Boundary and Operating Conditions

Saturated liquid water is entering into the heat sink at a constant saturation temperature (T_{in}) of 100°C and with an uniform velocity of (v_{in}) of 0.4 m/s, corresponding to 60 mL/min (i.e., mass flux, G=383.4 kg/m^2.s) of saturated liquid water flowing through the entire heat sink. Pressure outlet boundary condition is applied at all three outlets of the heat sink with gauge pressure of 0 Pa. No-slip velocity boundary condition is applied on all internal walls of the heat sink. The background and hotspot zones of the computational domain are subjected to non-uniform heat flux as explained in the Section II. Moreover, heat flux and temperature continuity conditions

Authorized licensed use limited to: Institut Teknologi Sepuluh Nopember. Downloaded on November 02,2026 at 03:10:37 UTC from IEEE Xplore. Restrictions apply.

are applied at all internal walls to ensure energy conservation across the solid and liquid domains. Finally, the two side walls of the computational domain are considered as symmetric, while all other external boundaries are assumed to be perfectly insulated.

Since the solid Si domain is expected to experience significant temperature gradients due to the non-uniform heat flux in the background and hotspot regions, temperature-dependent k of Si has been considered as follows [18]:

$$k_{Si} = 100\left(0.03 + \frac{1.56}{10^3}T + \frac{1.65}{10^6}T^2\right) \quad (15)$$

Where, the unit of T is Kelvin.

Table I summarizes all the thermo-physical properties used in this study. It is important to note that all properties of liquid water and water vapor are given at the saturation temperature of water of 100°C.

TABLE I: Thermo-physical properties of Si, liquid water and water vapor [18]

Property	Si	Liquid water	Water vapor
Density, ρ (kg/m^3)	2330	958.5	0.595
Thermal conductivity, k (W/m.K)	Eq. (15)	0.665	0.025
Specific heat, C_p (J/kg.K)	712	4217	2043
Dynamic viscosity, μ (mPa.s)	-	0.28	0.012
Surface tension coefficient, σ (N/m)	-	0.0589	
Latent heat of vaporization, h_{lv} (kJ/kg)	-	2257	

D. Numerical Scheme

The finite volume based CFD/HT solver ANSYS@ FLUENT@ 2021 R2 was used to numerically solve the discussed governing equations. The second-order upwind scheme was utilized to spatially discretize the momentum and energy equations. The SIMPLE algorithm was used for pressure and velocity coupling, and the gradients and pressure were discretized using the least squares cell-based method and PESTO scheme, respectively. The explicit VOF formulation with a first-order temporal discretization was employed, and the Courant number (Co) for the volume fraction equation was set to a cutoff value of 0.25. Geo-reconstruct scheme was utilized to discretize the face flux of the volume fraction. Moreover, depending on the mesh size and mass flux combinations, the time steps were automatically adjusted in the range of 10^{-8}–10^{-6} s to keep the global Co below a threshold limit of 0.9 for numerical stability. The solution was considered converged when the residuals for continuity and momentum equations were less than 10^{-4} and for the energy equation less than 10^{-7}, with 200 iterations per time step.

E. Solution Procedure

The converged single-phase steady-state solution for the velocity field corresponding to the given inlet velocity under isothermal condition at the specified saturation temperature of 100°C, was used as the initial condition for the flow boiling simulations.

The flow-boiling transient solution was reached to pseudo-steady-state conditions (i.e., negligible change in pressure drop and wall superheat between consecutive time steps) at ~40 ms. However, to enhance the stability and repeatability of the results, the transient simulations were run up to a flow time of 50 ms. It is important to note that for quantitative comparison, all transient numerical results are reported as average over a simulated flow time spanning from 40 ms to 50 ms.

F. Mesh Generation

An unstructured polyhedral conformal mesh has been generated using the ANSYS Fluent Meshing platform as shown in the Fig. 3. Moreover, three inflation layers have been generated over all solid-liquid interfaces to accurately resolve the transport quantities within the boundary layer. After sequential mesh independence analysis, 0.88M and 0.99M of mesh have been selected for the conventional microchannel and hybrid microchannel-pin fin heat sink layouts, respectively.

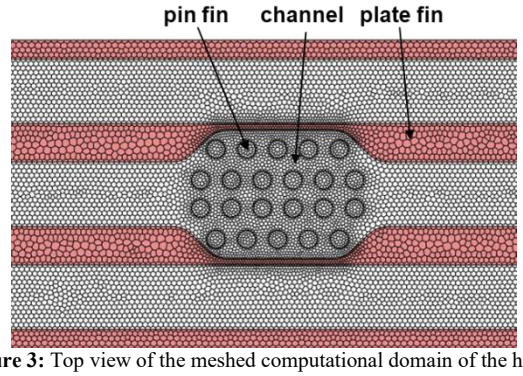

Figure 3: Top view of the meshed computational domain of the hybrid microchannel-pin fin heat sink.

G. Model Validation

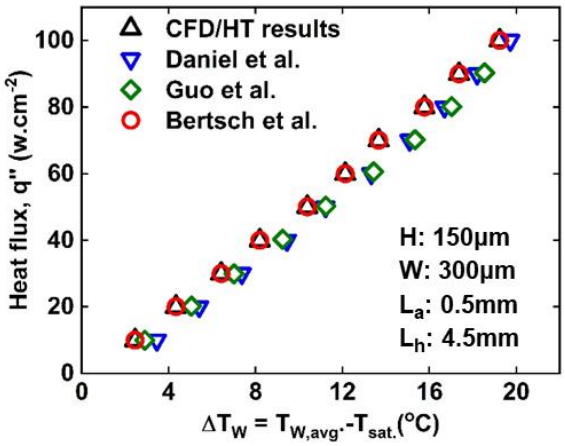

Figure 4: Comparison between the boiling curve obtained from the present CFD/HT flow boiling model, the numerical results reported by Daniel et al. [18] and Guo et al. [17], and the correlation proposed by Bertsch et al. [19]. Coolant mass flux and T_{in} were 500 kg/m^2.s and 373.15 K, respectively. For this validation, the transient flow boiling simulations were run for 20 ms, and for quantitative comparison, all reported numerical results are averaged over 10 ms to 20 ms.

Authorized licensed use limited to: Institut Teknologi Sepuluh Nopember. Downloaded on November 02,2026 at 03:10:37 UTC from IEEE Xplore. Restrictions apply.

In light of the absence of experimental data for the flow boiling microchannel heat sink with similar geometrical and operating conditions as the considered conventional and hybrid microchannel heat sinks, the developed CFD/HT model has been validated by comparing wall superheat (ΔT_w) variation with heat flux (q''), i.e., boiling curve with the numerical results reported by Daniel et al. [18] and Guo et al. [17] for a smooth microchannel formed by zero thickness wall with a cross-sectional area of 150 µm x 300 µm (height (H) x width (W)), an adiabatic entrance length (L_a) of 0.5 mm and a heated length (L_h) of 4.5 mm. To mimic the numerical results, saturated water has been considered as working fluid with a mass flux inlet boundary condition of G=500 kg/m^2.s and an uniform heat flux has been applied on the heated section of the microchannel. Moreover, the developed CFD/HT model has also been validated by comparing with the empirical correlation proposed by Bertsch et al. [19] for mini- and microchannels (see Fig. 4). From the figure, it can be seen that the developed CFD/HT model can very accurately predict the boiling curve compared to the other numerical results and empirical correlation over a wind range of input q'' conditions with a maximum ΔT_w difference of less than 2.1°C.

IV. Results and Discussion

A. Bubble Dynamics

Since in the flow boiling, vapor bubbles dictate the heat transfer behavior, spatio-temporal bubble dynamics have been studied for both heat sink layouts under different hotspot heat flux (q''_{hs}) conditions and presented in this section.

Figure 5 shows the temporal and spatial evolution of flow patterns for both the conventional microchannel and hybrid microchannel-pin fin heat sinks with a q''_{bg} of 30 W.cm^{-2} and q''_{hs} of 60 W.cm^{-2}. From the Fig. 5(a), it can be seen that initially at t=4 ms, bubble nucleation sites appear nearly everywhere inside the channels, however, vapor bubbles only coalescence and consequently grow larger at t=10 ms in the downstream of the microchannel heat sink. This behavior can be attributed to the gradually increasing wall superheat and bulk fluid temperature along the stream-wise direction of the heat sink. Moreover, up to t=10 ms, bubbles are smaller than the channel width, as shown in the Fig. 5(a), and the bubbly flow regime is primarily evident. Furthermore, at t=20 ms, bubbles started to coalescence more and grow larger from the side and bottom

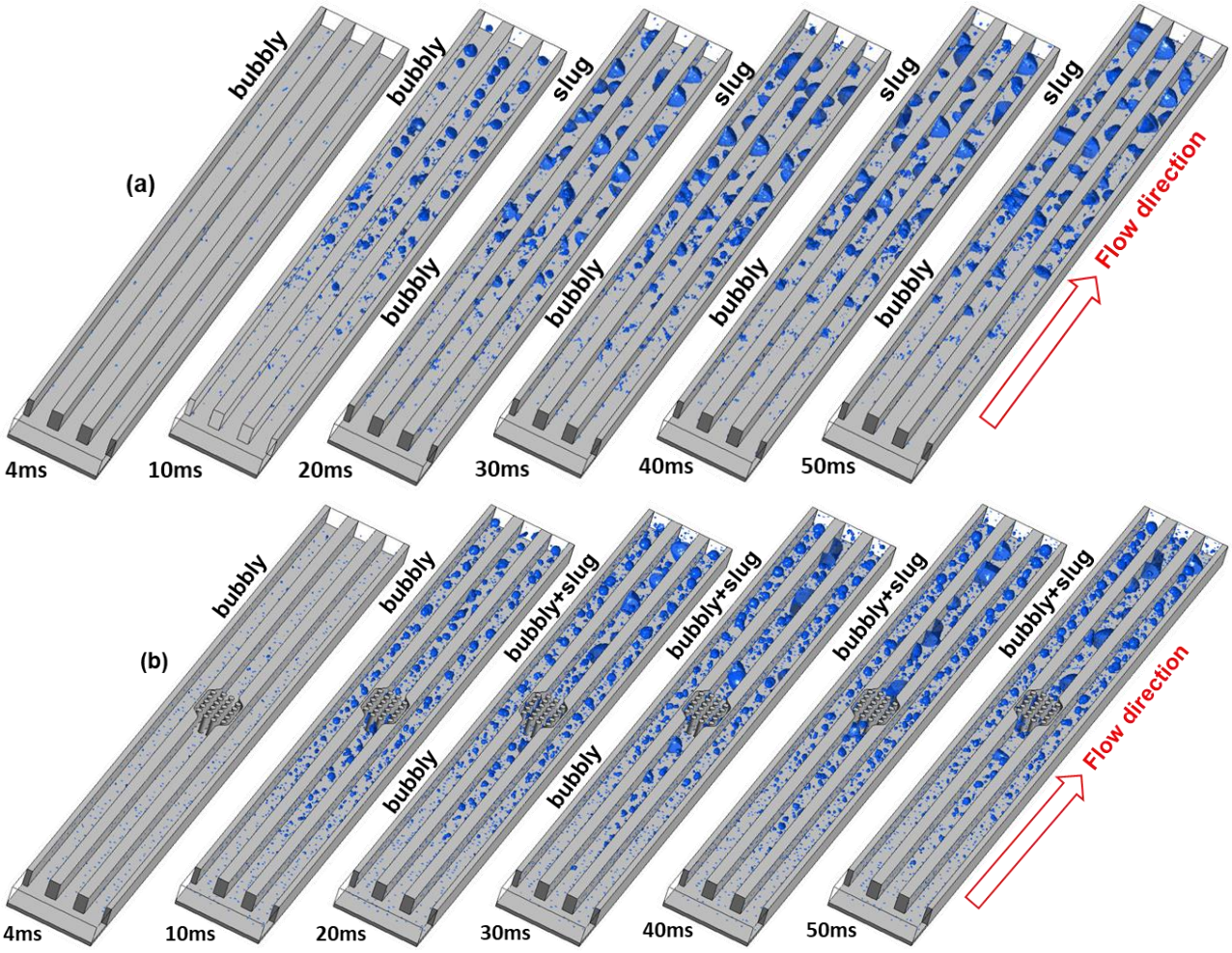

Figure 5: Temporal and spatial vapor distribution in (a) conventional microchannel and (b) hybrid microchannel-pin fin heat sinks with a q''_{bg} of 30 W.cm^{-2} and q''_{hs} of 60 W.cm^{-2}.

Authorized licensed use limited to: Institut Teknologi Sepuluh Nopember. Downloaded on November 02,2026 at 03:10:37 UTC from IEEE Xplore. Restrictions apply.

walls of the channels owing to the greater heat conduction through the solid domain, and subsequently, the flow regime in the downstream of the channels evolved into slug or coalescing bubbly flow. Afterward, at higher time steps of t=30 ms to 50 ms, large confined bubbles formed and their size gradually approached the channel width, especially in the downstream of the hotspot zone. It is worth mentioning that after t=40 ms, vapor bubble distribution remains virtually unchanged in both heat sinks, indicating a balance between vapor generation and removal rates, therefore reaching the quasi-steady state.

The hybrid microchannel-pin fin heat sink also shows very similar bubble dynamics such as similar bubble nucleation, coalescence phenomena, and flow regime as conventional microchannel heat sink, except slug flow is evident in the middle channel with larger bubbles, whereas bubbly flow with smaller bubbles generated in the two side channels (see Fig. 5(b)). In the case of hybrid microchannel-pin fin heat sink, clustered pin fins inside the middle channel result in significantly high flow resistance across this channel and consequently, lower coolant flow rate compared to the side channels. For example, at t=50 ms, mass flux (G) through the middle channel is ~44% lower than two side channels. Moreover, stagnation regions inside the clustered pin fins act as bubble nucleation sites, which eventually enhance boiling inside the middle channel, as shown in the Fig. 5(b). These combined effects of lower coolant flow through the middle channel and more nucleation sites result in larger bubbles in the middle channel and smaller bubbles in the side channels.

Figure 6 shows the spatio-temporal evolution of flow patterns for both the conventional microchannel and hybrid microchannel-pin fin heat sinks with a q''_{bg} of 30 W.cm^{-2} and q''_{hs} of 120 W.cm^{-2}. From the figure, it can be seen that both heat sinks show very similar bubble dynamics and boiling regimes as low q''_{hs}, except more bubble nucleation in the downstream of the hotspot region and subsequently slightly higher vapor volume fraction, which can be attributed to the high wall superheat under higher q''_{hs} and low coolant flow through the middle channel.

Overall, bubbly and slug flow regime was evident in the upstream and downstream of both the heat sinks with any operating condition, and the hotspot doesn't have any significant effect on the bubble distribution and the corresponding boiling regime.

Figure 7 presents the temporal variation of % of vapor volume fraction for both the conventional and hybrid microchannel-pin fin heat sinks under different heterogeneous heat flux conditions. For both heat sink layouts and heat flux

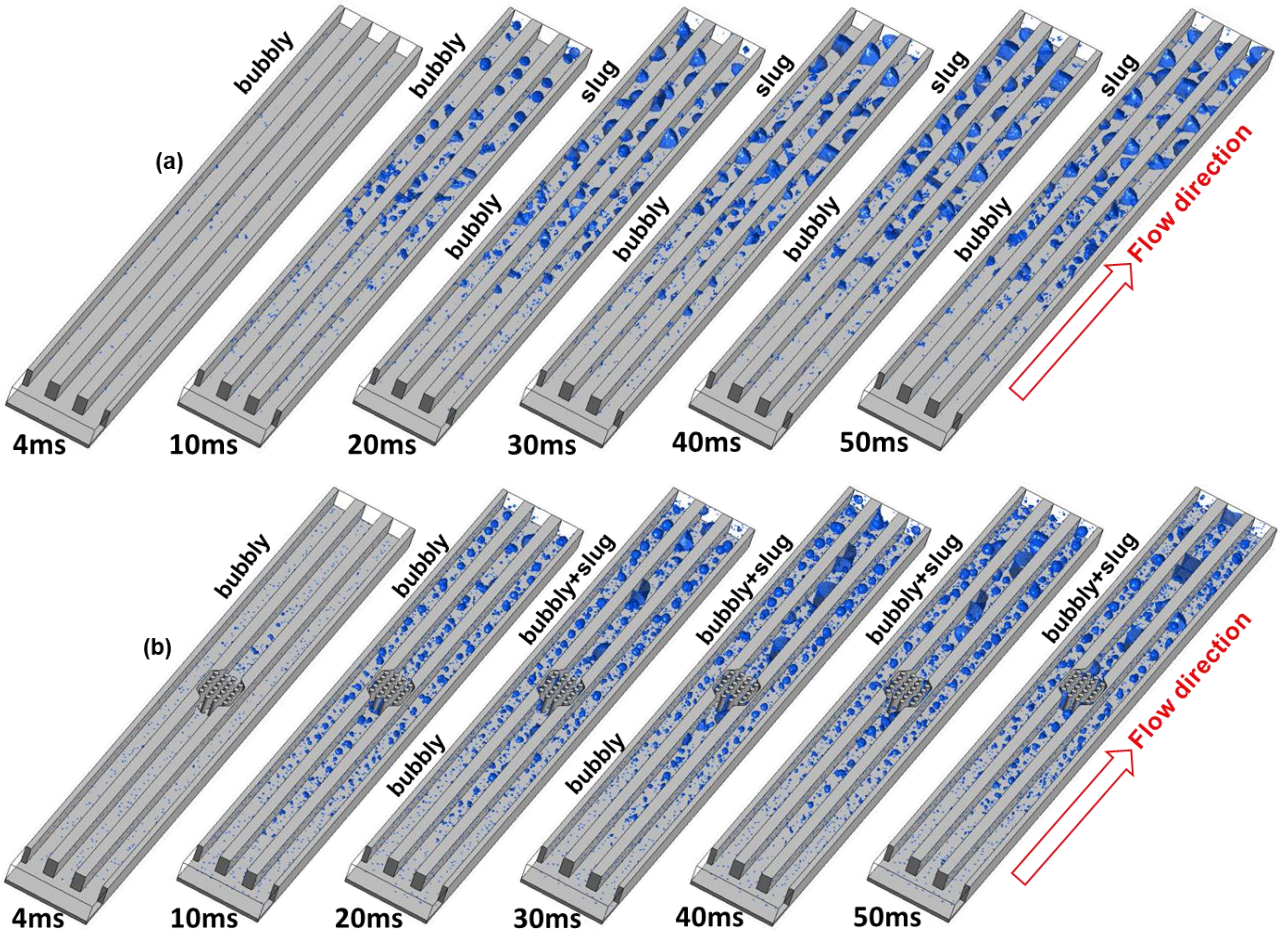

Figure 6: Temporal and spatial vapor distribution in (a) conventional microchannel and (b) hybrid microchannel-pin fin heat sinks with a q''_{bg} of 30 W.cm^{-2} and q''_{hs} of 120 W.cm^{-2}.

Authorized licensed use limited to: Institut Teknologi Sepuluh Nopember. Downloaded on November 02,2026 at 03:10:37 UTC from IEEE Xplore. Restrictions apply.

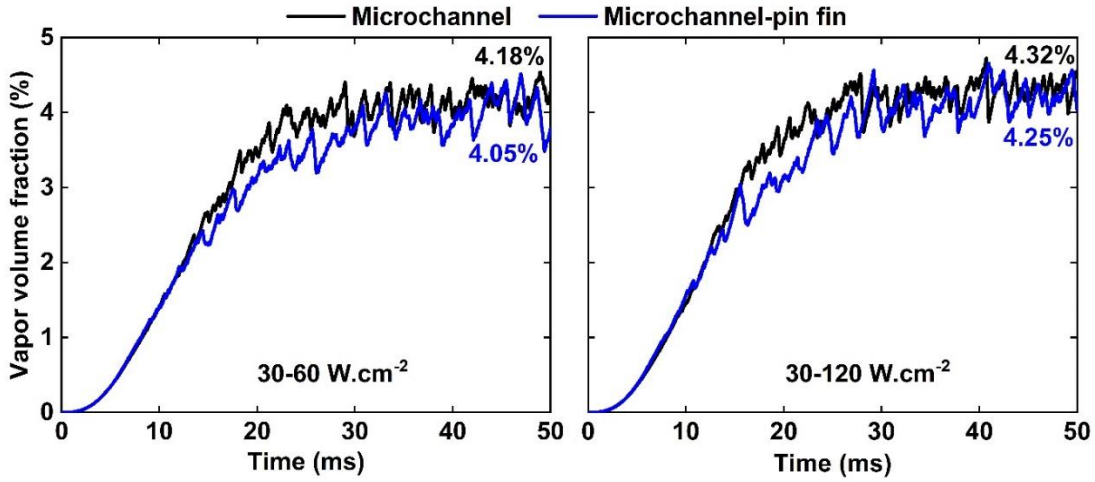

Figure 7: Temporal variation of % of vapor volume fraction. For quantitative comparison, reported numerical results are averaged over 40 ms to 50 ms.

conditions, vapor volume fraction gradually increases with time and eventually reaches to quasi-steady-state condition at ~40 ms, as shown in the Fig. 7. Interestingly, hybrid microchannel-pin fin heat sink generates slightly lower vapor fraction compared to the conventional microchannel heat sink owing to the enhanced thermal performance of the hybrid heat sink which will be explained in the next Section. For instance, at q''_{bg} of 30 W.cm^{-2} and q''_{hs} of 60 W.cm^{-2} and 120 W.cm^{-2}, the hybrid heat sink generates ~3% and 1.6% lower vapor compared to the conventional microchannel heat sink, respectively.

B. Thermal Performance

Figure 8 presents the spatio-temporal temperature evolution of the heated bottom surface of both heat sink layouts at q''_{bg} of 30 W.cm^{-2} and q''_{hs} of 60 W.cm^{-2}. From the figure, it can be seen that up to 10 ms, both heat sink provides very uniform temperature distribution across the full domain owing to bubbly flow boiling regime, as explained in the Fig. 5. In the case of conventional microchannel heat sink, large confined bubbles, i.e., slug flow (see Fig. 5) in the downstream of the hotspot region results in significantly high temperature at t=20 ms, as shown in the Fig. 8(a). Moreover, from t=30 ms to onward, substrate temperature gradually increases along the stream-wise direction from the inlet to the outlet, especially after the hotspot region, which can be attributed to the gradually increasing slug flow dominance. After t=40 ms, the temperature distribution remains virtually unchanged indicating the so-called quasi-steady state. Interestingly, at q''_{hs} of 60 W.cm^{-2} and in the case of conventional microchannel heat sink, substrate temperature at the rear of the heat sink is higher than the hotspot (see Fig. 8(a)) temperature.

The hybrid microchannel-pin fin heat sink demonstrates a substantial decrease in both hotspot and background temperatures when compared to the conventional microchannel heat sink, as evident in the Fig. 8(b). The presence of clustered

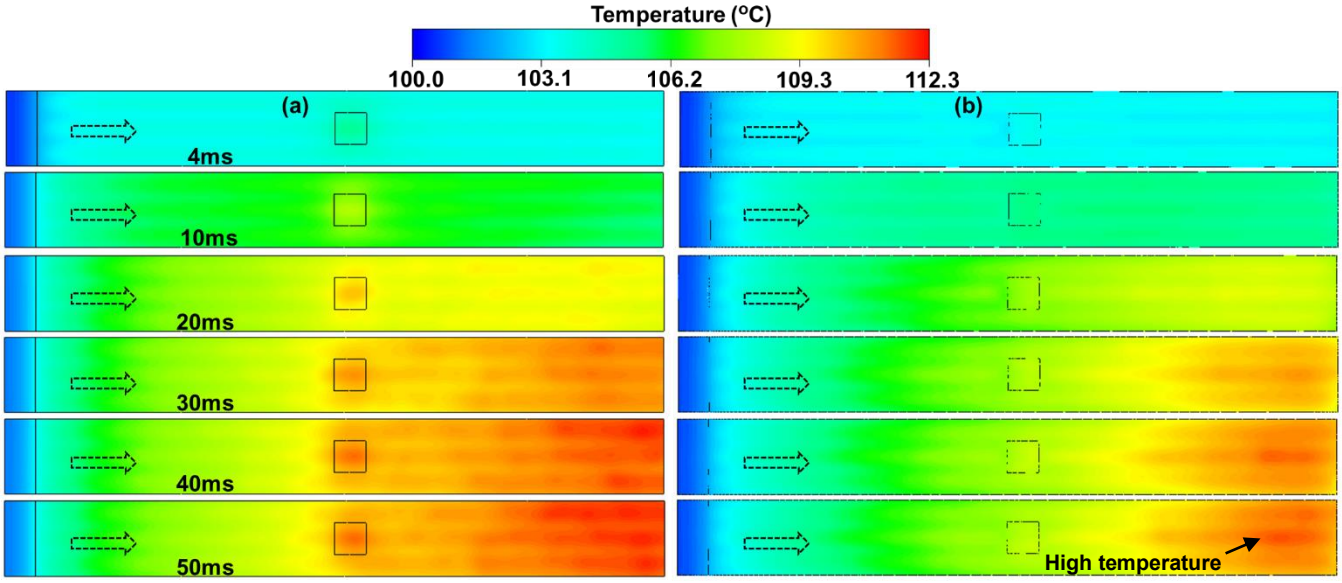

Figure 8: Temporal and spatial temperature distribution at the bottom surface (x-z plane at y = 0) of the (a) conventional microchannel and (b) hybrid microchannel-pin fin heat sinks with a q''_{bg} of 30 W.cm^{-2} and q''_{hs} of 60 W.cm^{-2}.

Authorized licensed use limited to: Institut Teknologi Sepuluh Nopember. Downloaded on November 02,2026 at 03:10:37 UTC from IEEE Xplore. Restrictions apply.

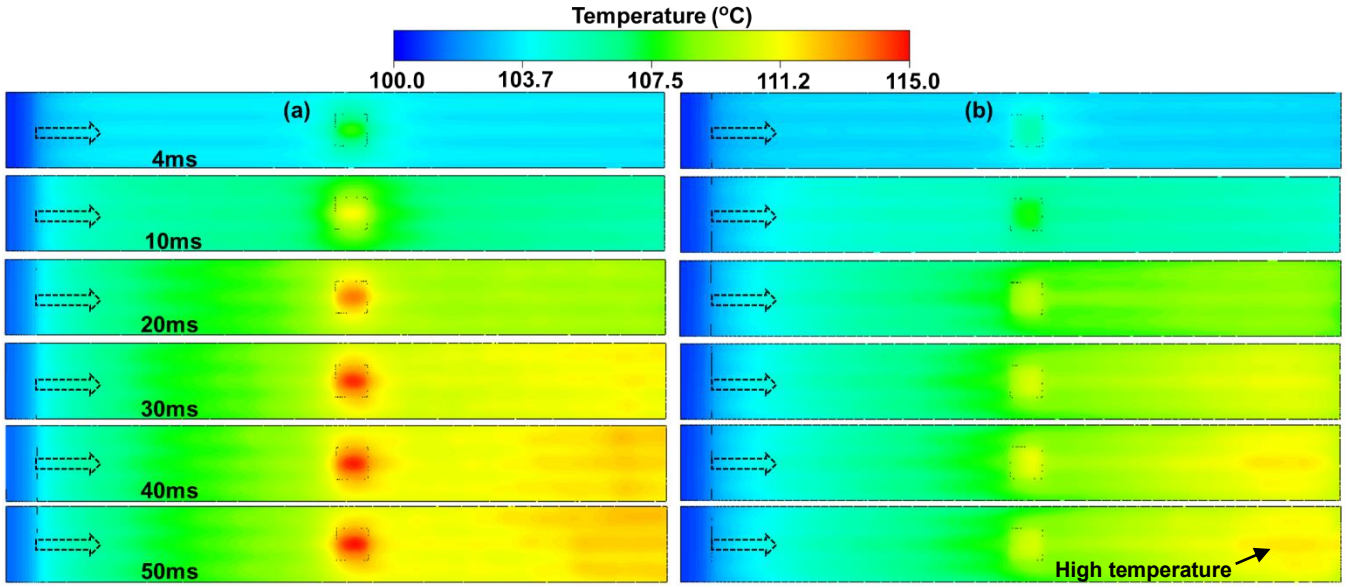

Figure 9: Temporal and spatial temperature distribution at the bottom surface (x-z plane at y = 0) of the (a) conventional microchannel and (b) hybrid microchannel-pin fin heat sinks with a q''_{bg} of 30 W.cm^{-2} and q''_{hs} of 120 W.cm^{-2}.

pin fins over the hotspot region significantly augments the heat transfer area, leading to a notable reduction in hotspot temperature. On the contrary, the heightened flow resistance induced by pin fins in the middle channel results in increased coolant flow through the side channels, enhancing convection heat transfer and promoting bubbly flow in these channels, which eventually reduces the background temperature as shown in the Fig. 8(b). However, reduced coolant flow through the middle channel provides higher temperature downstream of the hotspot in the middle channel owing to the large confined bubbles, i.e., plug flow regime as explained previously (see Fig. 8(b)).

Similar spatio-temporal temperature distribution is evident in the Fig. 9 for both heat sink layouts at q''_{bg} of 30 W.cm^{-2} and q''_{hs} of 120 W.cm^{-2}, except in the case of conventional microchannel heat sink, hotspot temperature is significantly higher than the substrate temperature and heat spreading from the hotspot zone is more profound at high q''_{hs} in both the span and stream-wise direction (see Fig. 9(a)).

Figure 10 presents the temporal variation of peak temperature for both the conventional microchannel and hybrid microchannel-pin fin heat sinks under different heterogeneous heat flux conditions. Irrespective of heat sink layouts and heat flux conditions, the temperature of both heat sinks gradually increase over time and eventually reaches the quasi-steady-state conditions at ~40 ms (see Fig. 10). From the figure, it can be seen that at q''_{bg} of 30 W.cm^{-2} and q''_{hs} of 60 W.cm^{-2} and 120W.cm^{-2}, the hybrid heat sink effectively reduces the peak hotspot temperature by ~3°C and 4°C, respectively, compared to the conventional microchannel heat sink. Furthermore, in the case of hybrid microchannel-pin fin heat sink, peak quasi-steady-state temperature of the background is higher than the hotspot at both heating conditions. This can be attributed to the locally enhanced heat transfer area over the hotspot region which leads to significant reduction in hotspot temperature, and reduced coolant flow through the middle channel which results

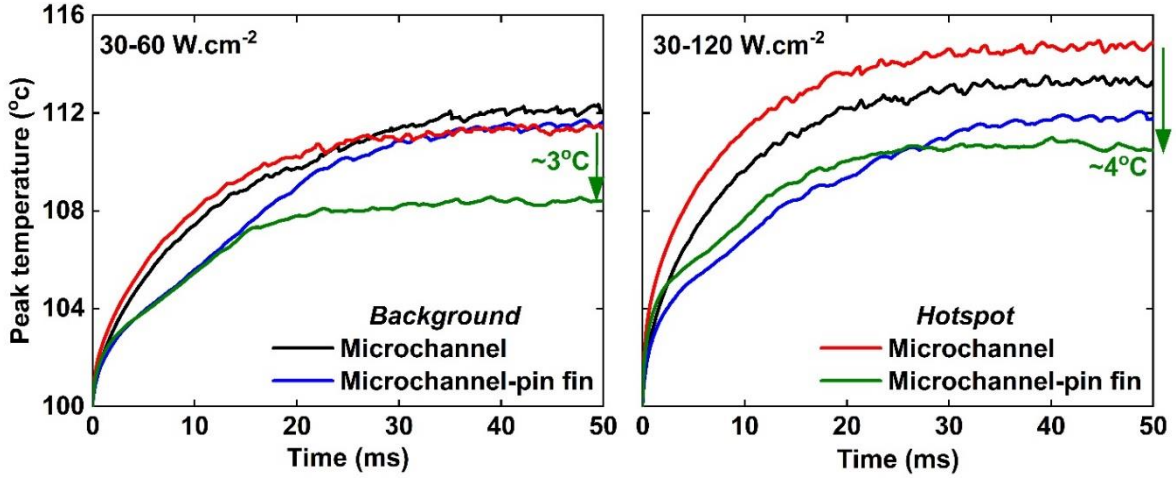

Figure 10: Temporal variation of peak temperature at different heterogeneous heat flux conditions. For quantitative comparison, reported numerical results are averaged over 40 ms to 50 ms.

Authorized licensed use limited to: Institut Teknologi Sepuluh Nopember. Downloaded on November 02,2026 at 03:10:37 UTC from IEEE Xplore. Restrictions apply.

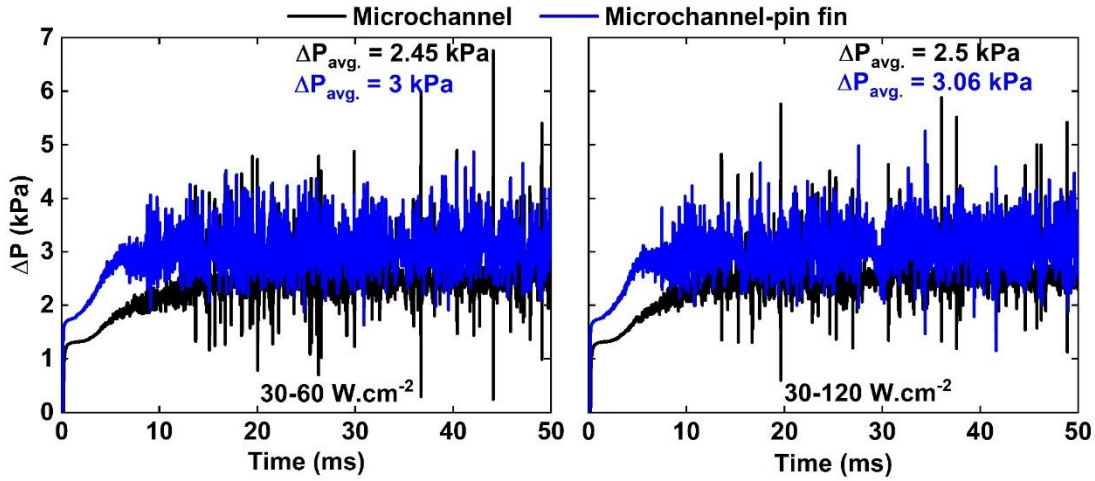

Figure 11: Temporal variation of flow boiling pressure drop at different heterogeneous heat flux conditions. For quantitative comparison, reported numerical results are averaged over 10 ms to 50 ms.

in large confined bubbles and plug flow regime in the downstream of the hotspot region.

C. *Pressure Drop Characteristics*

The temporal variation in the flow boiling pressure drop (ΔP) is plotted in Fig. 11 for both the heat sink layouts and heat flux conditions. As shown, ΔP reaches the pseudo-steady-state conditions at ~10 ms for both heat sink layouts and heating conditions. Moreover, in the case of hybrid heat sink, ΔP is ~0.55 kPa higher than the conventional heat sink at both heating conditions, which can be attributed to the increased flow resistance induced by the clustered pin fins in the middle channel. Although continuous change in the vapor generation results in significantly fluctuating ΔP irrespective of the heat sink layouts and heat fluxes, the hybrid heat sink provides relatively small pressure fluctuation compared to the conventional microchannel heat sink owing to the enhanced bubble dynamics, i.e., dominant bubbly flow regime as previously explained. From the Fig. 11, it can also be seen that ΔP increases slightly with q''_{hs}. This could be due to high bubble generation at higher q''_{hs} and consequently, high flow resistance.

V. CONCLUSIONS

In this paper, a hybrid microchannel-pin fin heat sink layout has been proposed to enhance the temperature non-uniformity under heterogeneous heating conditions with a minimal pumping cost by locally increasing the heat transfer area using clustered pin fins only over the hotspot zones. A coupled 3D volume-of-fluid (VOF) and phased-change model has been developed to assess the thermal-hydraulic performance of the proposed hybrid microchannel-pin fin heat sink under flow boiling conditions using saturated water as coolant. The flow boiling performance of the hybrid microchannel-pin fin heat sink has also been benchmarked with the conventional microchannel heat sink. Based on the numerical results, the following conclusions can be drawn:

1. Bubbly and slug flow regimes were primarily evident in the upstream and downstream of both conventional microchannel and hybrid microchannel-pin fin heatsinks, respectively. Moreover, the hotspot region has negligible effect on the bubble distribution and the corresponding boiling regime.
2. The hybrid microchannel-pin fin heat sink generates a slightly lower vapor fraction compared to the conventional microchannel heat sink owing to the enhanced thermal performance of the hybrid heat sink.
3. The hybrid microchannel-pin fin heat sink significantly reduces the hotspot temperature and provides enhanced temperature uniformity compared to the conventional microchannel heat sink. However, both heat sink layouts suffer from a noticeable temperature gradient in the rear section of the heat sinks.
4. The hybrid microchannel-pin fin heat sink exhibits a marginally higher pressure drop than the conventional microchannel heat sink due to the increased flow resistance induced by the clustered pin fins in the middle channel.

ACKNOWLEDGMENT

This research was supported in part through research cyberinfrastructure resources and services provided by the Partnership for an Advanced Computing Environment (PACE) at the Georgia Institute of Technology, Atlanta, Georgia, USA.

REFERENCES

[1] A. Tikadar et al., "Enhancing thermal-hydraulic performance of counter flow mini-channel heat sinks utilizing secondary flow: Numerical study with experimental validation," International Communications in Heat and Mass Transfer, vol. 111, p. 104447, 2020/02/01/ 2020.

[2] A. Tikadar et al., "Parametric study on thermal and hydraulic characteristics of inter-connected parallel and counter flow mini-channel heat sink," Applied Thermal Engineering, vol. 153, pp. 15-28, 2019/05/05/ 2019.

[3] M. B. Bowers and I. Mudawar, "High flux boiling in low flow rate, low pressure drop mini-channel and micro-channel heat sinks," International Journal of Heat and Mass Transfer, vol. 37, no. 2, pp. 321-332, 1994/01/01/ 1994.

Authorized licensed use limited to: Institut Teknologi Sepuluh Nopember. Downloaded on November 02,2026 at 03:10:37 UTC from IEEE Xplore. Restrictions apply.

[4] T. Chen and S. V. Garimella, "Measurements and high-speed visualizations of flow boiling of a dielectric fluid in a silicon microchannel heat sink," International Journal of Multiphase Flow, vol. 32, no. 8, pp. 957-971, 2006/08/01/ 2006.

[5] T. Chen and S. V. Garimella, "Local heat transfer distribution and effect of instabilities during flow boiling in a silicon microchannel heat sink," International Journal of Heat and Mass Transfer, vol. 54, no. 15, pp. 3179-3190, 2011/07/01/ 2011.

[6] X. Ma et al., "Flow boiling instability and pressure drop characteristics based on micro-pin-finned surfaces in a microchannel heat sink," International Journal of Heat and Mass Transfer, vol. 195, p. 123168, 2022/10/01/ 2022.

[7] S. K. Oudah et al., "An experimental investigation of the effect of multiple inlet restrictors on the heat transfer and pressure drop in a flow boiling microchannel heat sink," International Journal of Heat and Mass Transfer, vol. 153, p. 119582, 2020/06/01/ 2020.

[8] T. Alam, P. S. Lee, and C. R. Yap, "Effects of surface roughness on flow boiling in silicon microgap heat sinks," International Journal of Heat and Mass Transfer, vol. 64, pp. 28-41, 2013/09/01/ 2013.

[9] E. Sourtiji and Y. Peles, "Flow boiling in microchannel with synthetic jet in cross-flow," International Journal of Heat and Mass Transfer, vol. 147, p. 119023, 2020/02/01/ 2020.

[10] W. Qu and I. Mudawar, "Flow boiling heat transfer in two-phase micro-channel heat sinks—I. Experimental investigation and assessment of correlation methods," International Journal of Heat and Mass Transfer, vol. 46, no. 15, pp. 2755-2771, 2003/07/01/ 2003.

[11] A. Kalani and S. G. Kandlikar, "Combining liquid inertia with pressure recovery from bubble expansion for enhanced flow boiling," Applied Physics Letters, vol. 107, no. 18, p. 181601, 2015.

[12] D. Lorenzini and Y. Joshi, "Numerical modeling and experimental validation of two-phase microfluidic cooling in silicon devices for vertical integration of microelectronics," International Journal of Heat and Mass Transfer, vol. 138, pp. 194-207, 2019/08/01/ 2019.

[13] D. Lorenzini and Y. Joshi, "Flow boiling heat transfer in silicon microgaps with multiple hotspots and variable pin fin clustering," Physics of Fluids, vol. 31, no. 10, p. 102002, 2019.

[14] D. Ansari and K.-Y. Kim, "Hotspot thermal management using a microchannel-pinfin hybrid heat sink," International Journal of Thermal Sciences, vol. 134, pp. 27-39, 2018/12/01/ 2018.

[15] A. Tikadar and S. Kumar, "Local hotspot thermal management using metal foam integrated heat sink," Applied Thermal Engineering, vol. 221, p. 119632, 2023/02/25/ 2023.

[16] B. Arkles, "Hydrophobicity, hydrophilicity and silanes," Paints Coat. Ind., vol. 22, p. 114-135, 2023.

[17] Y. Guo et al., "Numerical simulation of flow boiling heat transfer in microchannel with surface roughness," International Journal of Heat and Mass Transfer, vol. 204, p. 123830, 2023/05/01/ 2023.

[18] D. Lorenzini and Y. K. Joshi, "Computational Fluid Dynamics Modeling of Flow Boiling in Microchannels With Nonuniform Heat Flux," Journal of Heat Transfer, vol. 140, no. 1, 2017.

[19] S. S. Bertsch, E. A. Groll, and S. V. Garimella, "A composite heat transfer correlation for saturated flow boiling in small channels," International Journal of Heat and Mass Transfer, vol. 52, no. 7, pp. 2110-2118, 2009/03/01/ 2009.

Authorized licensed use limited to: Institut Teknologi Sepuluh Nopember. Downloaded on November 02,2026 at 03:10:37 UTC from IEEE Xplore. Restrictions apply.